Journal of Alloys and Compounds 509 (2011) 4748–4753

Contents lists available at ScienceDirect

Journal of Alloys and Compounds

journal homepage: www.elsevier.com/locate/jallcom

Magnetic annealing effects on multiferroic $BiFeO_3/CoFe_2O_4$ bilayered films

Xianwu Tang[a], Jianming Dai[a], Xuebin Zhu[a,*], Wenhai Song[a], Yuping Sun[a,b]

[a] Key Laboratory of Materials Physics, Institute of Solid State Physics Hefei 230031, PR China
[b] High Magnetic Field Laboratory, Chinese Academy of Sciences, Hefei 230031, PR China

ARTICLE INFO

Article history:
Received 5 January 2011
Accepted 21 January 2011
Available online 2 February 2011

PACS:
81.40.Wx
81.10.Dn
68.55.−a
75.70.−i
77.84.−s

Keywords:
$BiFeO_3$
$CoFe_2O_4$
Bilayered films
Magnetic annealing
Magnetoelectric effect

ABSTRACT

In situ magnetic annealing effects on *c*-axis-preferred multiferroic $BiFeO_3/CoFe_2O_4$ bilayered by chemical solution deposition route are investigated. It is observed that magnetic annealing can enhance the crystallization quality, texture and densification as well as dielectric properties. In addition, the magnetolosses decrease with increasing the magnetic fields. Moreover, both increase of the polarization and decrease of the leakage current due to magnetic annealing are beneficial for potential applications of $BiFeO_3$ films.

1. Introduction

$BiFeO_3$ (BFO) is one of the most important multiferroics in the views of the applications perspective and engineering possibilities [1,2]. Highly ferroelectric ordering temperature and magnetic ordering temperature make it as an attractive candidate for bifunctional device applications in the emerging field of spintronics [3]. Although BFO thin films exhibit excellent ferroelectric properties, the weak magnetic behavior and considerable high leakage current limit their multifunctional applications. In addition, the coupling of the electric and magnetic polarizations provides an additional degree of freedom in device design [4] and large magnetoelectric behavior is needed in the view of application. One hand, the highly preferred (0 0 1)-oriented BFO thin films have the large magnetoelectric effect, which is reported by our previous works [5]. On the other hand, multilayered structure with ferrimagnetic layer is also an approach to get large magnetoelectric behavior. Furthermore, the multilayered structure approach is among the most promising ongoing topics, whereby the coupling and interactions among the different functional layers can strongly be influenced by two factors. One is the physical property of each single layer thin film. For multiferroic applications, the spinel $CoFe_2O_4$ (CFO) is a predominant ferrimagnetic material with large magnetostriction and high Curie temperature [6,7]. The other factor is the preparing method. The properties of thin films depend on the microstructure and texture of the films, which in turn are strongly determined by the processing parameters of preparation. Magnetic field, as the unique physical properties of magnetic materials, is recognized not only as a parameter for studying the physical properties but also as a tool to synthesize materials [8]. It has been already found that the application of external magnetic fields during the process of materials synthesis can play an important role in affecting the texture, microstructure, grains size, defects and magnetic properties of final materials [9–14]. Improvement in magnetic and electric properties of BFO ceramic with high magnetic field annealing has been reported [15]. Investigation of magnetic annealing effects on the BFO thin films prepared via chemical solution deposition (CSD) method will be reported in our other works. In recent, there are some reports about the pulse laser deposition (PLD)-derived CFO/BFO bilayered films [16,17]. However, there are rarely any reports about the preparing BFO/CFO bilayered thin films via CSD method. Additionally, compared with the properties of PLD-derived BFO thin films, although the CSD approach has several advantages for film preparation such as strict control of stoichiometry, easy processing for large-area films on complex-shaped substrates and low-cost for the products, there are still some defects in CSD-

* Corresponding author.
E-mail addresses: jmdai@issp.ac.cn (J. Dai), xbzhu@issp.ac.cn (X. Zhu).

0925-8388/$ – see front matter © 2011 Elsevier B.V. All rights reserved.
doi:10.1016/j.jallcom.2011.01.143

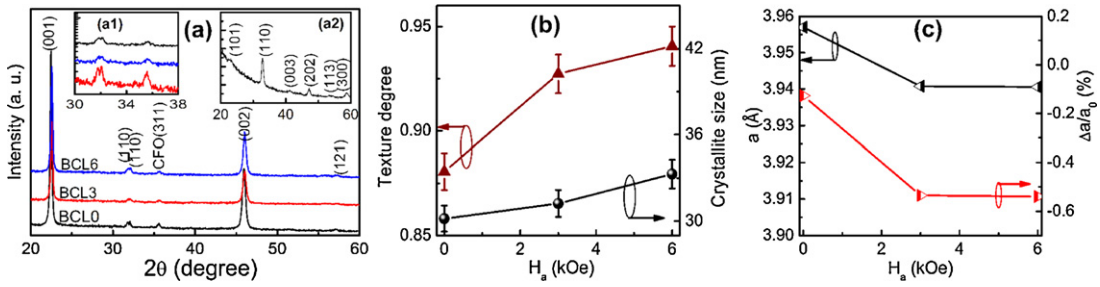

Fig. 1. (a) X-ray diffractometer for the bilayered BFO/CFO thin films annealed under different applied magnetic fields. A magnified diffraction pattern between 30° and 38° of 2θ is shown in the inset of (a1). XRD of the single-layered LNO films is shown in the inset of (a2). (b) The variation of texture degree and crystalline sizes of the films with magnetic annealing field. (d) Variation in the lattice constant a and percentage lattice parameter change $\Delta a/a_0$ % of BFO films with varying annealing field.

derived BFO based thin films, for example, large leakage current, poor densification. Many works have been reported to decrease the leakage current of CSD-derived BFO thin films though Bi-site or Fe-site substitution or co-doping with other elements [18,19]. However, in our previous works, it was observed that the ferroelectric properties and densification of the BFO thin films have been enhanced with magnetic annealing route.

In this work, c-axis-oriented bilayered BFO/CFO thin films were prepared on $LaNiO_3$ (LNO)-buffered silicon substrate with magnetic annealing process. The magnetic annealing effects on the grain growth, magnetic, dielectric, ferroelectric properties as well as magnetoelectic effect of the films are investigated.

2. Experimental procedure

Each layer of the BFO/CFO bilayered thin films, including the LNO layer, was fabricated on the n-typed (1 0 0)-oriented Si substrate via CSD methods. The LNO electrode layer was prepared with improved precursor solution based on the technique as described elsewhere [20] on the Si substrate etched with HF acid (10% in concentration). The LNO films were a thickness of 50 nm with resistivity of a magnitude of 10^{-4} Ωccm. Next, iron nitrate enneahydrate ($Fe(NO_3)_3{\cdot}9H_2O$, 99.99% in purity), Cobaltous acetate ($Co(CH_3COO)_2{\cdot}4H_2O$, 98% in purity), 2-methoxyethanol and acetic acid were used as the starting materials for preparing the CFO layer. The CFO layer was deposited on the LNO layer with rotation speed of 5000 rpm, 30 s, pyrolysis at 300 °C, 10 min in air and repeating 2 times, then crystallized at 650 °C in air for 1 h. The thickness of CFO layer was about 50 nm. Finally, BFO thin films were prepared by our previous reported ways [5] with the layer thickness about 270 nm. The external magnetic fields ($0\,\text{Oe} \leqslant H \leqslant 7\,\text{kOe}$) produced by water-cooled magnet were applied to parallel to the films surface during the BFO annealing process. For the sake of description, the sample prepared under 0, 3 and 6 kOe magnetic field is defined as BCL0, BCL3 and BCL6, respectively.

A Philips X'pert PRO X-ray diffractormeter (XRD) with Cu Kα radiation was used to check up crystallization quality and out-of-plane orientation of the films. Field-emission scanning electronic microscopy (FE-SEM, FEI Sirion 200 type, FEI, Hillsboro, Oregon USA) fitted with an energy dispersive X-ray analyzer (EDX) was used to detect the surface morphologies, thickness as well as the element composition. Magnetic properties were measured on a quantum design superconducting quantum interference device (SQUID, MPMS XL5 type) ($1.8\,\text{K} \leqslant T \leqslant 400\,\text{K}$, $0\,\text{T} \leqslant H \leqslant 5\,\text{T}$). Top Pt electrodes are deposited by sputtering on the surface of BFO layer with Miriam small ion sputtering (SCB-12) and the LNO layer was used as bottom electrodes. Dielectric response was investigated with LCR meter (TH2828/A/S) at room temperature. The ferroelectric properties and leakage current were investigated using a Sawyer–Tower circuit attached to a computer-controlled standardized ferroelectric test system (Radiant Technology 609B). Magnetoelectric effects were determined by measuring the variation of room temperature dielectric responses of the films with magnetic fields produced by the SQUID at the frequency of 1 MHz.

3. Result and discussion

The standard XRD $\theta - 2\theta$ patterns of CSD-derived BFO/CFO bilayered thin films annealing under different magnetic fields are shown in Fig. 1(a). It can be observed that all samples are single-phase without any undesirable phases. All the BFO diffraction peaks can be indexed in rhombohedrally distorted perovskite structure with space group $R3c$. All the BFO layers of the samples present a (0 0 1)-preferred orientation. In order to give a clear image, the magnified diffraction pattern between 30° and 38° of 2θ is shown in the inset (a1) of Fig. 1(a) within semi-log scale. The diffraction peaks come from non-preferred LNO layer are lost in the background due to its weak peak intensity, while the XRD of the single layered LNO/Si thin films is shown in the inset (a2) of Fig. 1(a). The compositions obtained from the EDX spectrum of the films, which is not shown here, indicated a Bi:Fe:Co ratio of 3.10:5.09:1.

With the purpose of investigating the magnetic annealing effects on the orientation and crystallite growth of the bilayered films, the BFO crystallite size and the c-axis texture degree is calculated respectively, and the results are shown in Fig. 1(b). It is observed that BFO crystallite size calculated with Scherrer formula of all the samples is about 32 nm, which does not show much change with increasing the magnetic fields. However, the texture degree calculated by Lotgering factor method [21] is improved from 0.87 for non-field annealing BCL0 to 0.94 for the 6 kOe field annealing BCL6. The enhancement in texture is attributed to two factors. One is the self-oriented growth behavior resulting from rapid thermal processing and {0 0 1} surface being the lowest energy surface as our previous report [5]. The other is that the easy magnetization axis of BFO is lying in the (0 0 1) plane [22]. The BFO (0 0 1) plane will grow in order to decrease the free energy [9] induce by magnetic annealing as discussed below, which results in texture degree increasing.

In consideration of existing large misfit in magnetostriction coefficient between BFO and CFO, the strain induced by the CFO layer must be different with the different magnetic field annealing process. Thus, the lattice constant a of the BFO (0 0 1) plane is calculated and the percentage change in lattice constant ($(a - a_0)/a_0$ %) versus applied annealing field (H_a) are plotted in Fig. 1(c), where a_0 is taken as 3.97 Å [23]. It shows the lattice constant decreases from 3.957 Å (BCL0) to 3.941 Å (BCL3) and to 3.939 Å (BCL6). The value of the percentage changed in lattice constant decrease from −0.127% (BCL0) to −0.539% (BCL3) and to −0.541% (BCL6), which suggests the strain of (0 0 1) plane increases with increasing the annealing magnetic field.

To further investigate the effects of the magnetic annealing on the microstructure of the films, surface FE-SEM is carried out and the results are shown in Fig. 2(a)–(c). Two clear interface layers are observed between the BFO, CFO and LNO layers from the cross FE-SEM image, as shown in Fig. 2(d). It is also observed that the grain boundaries reduce and become blurred with increasing the applied magnetic field. As it is well known, materials will be affected by magnetic fields due to magnetization force. For magnetic materials and paramagnetic materials, it is pulling force, on the contrary it is repulsing one for diamagnetic materials [13]. The forces can improve the connection and diffusion of components, which will result in improving the grain connectivity and densification of the materials. The driving force for grain growth p_m due to the magnetic field is given by the difference of magnetic energies of the adjacent grains with different orientations: $p_m = \mu_0 \Delta\chi H^2(\cos\theta_1 - \cos\theta_2)/2$, where μ_0 is the vacuum permeability, H is the applied magnetic

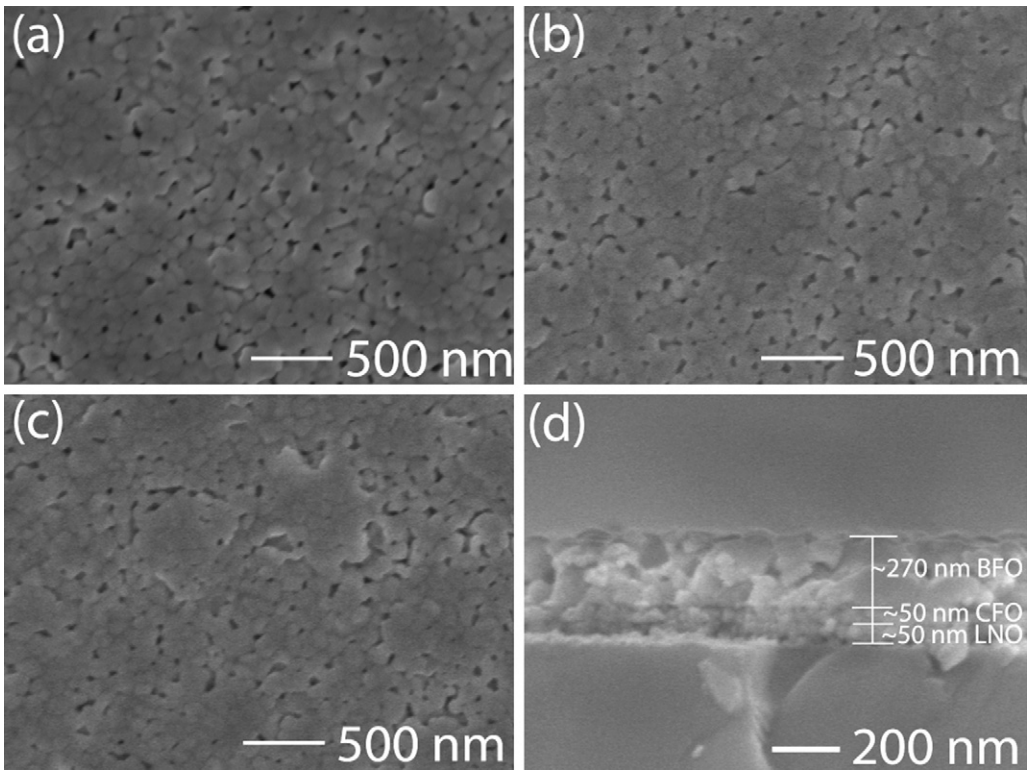

Fig. 2. The surface FE-SEM images of the films. (a) BCL0; (b) BCL3; (c) BCL6. The cross FE-SEM image of the typical films of BCL6.

field strength, and $\Delta\chi$ is the difference of the magnetic susceptibilities parallel and perpendicular to the easy magnetization axis, and θ_1, θ_2 are the angles between the direction of the magnetic field and the easy magnetization axis of both adjacent crystallites[12]. For BFO, its easy magnetization axis is lying in the (0 0 1) plane and the applied annealing magnetic fields parallel to the films surface. The magnetic force will drive the BFO grain boundary diffusing growing along and force the BFO (0 0 1) plane paralleling to the direction of the annealing field in order to decrease the free energy. As a result, the texture and grain size as well as densification of the films increase with magnetic annealing, as shown in Figs. 1(b) and 2, respectively.

To study magnetic annealing effects on the dielectric properties of the films, relative permittivity (ε_r) and tangent loss (tanδ) of the different magnetic field annealing BFO/CFO bilayered films as a function of frequency at room temperature are shown in Fig. 3(a) and inset of Fig. 3(a), respectively. It can be observed that the relative permittivity and the tangent loss of the films drastically decrease with increasing frequency at low frequency and approach a nearly steady-state value at high frequencies. The general decrease in relative permittivity with increasing frequency is expected for the dielectric thin film and in agreement with those published previously for BFO [24,25] and CFO [26,27]. The relative permittivity and tangent loss of the bilayered films increases and decreases with increasing the magnetic annealing field, respectively. In order to know the dielectric contribution of each sublayer of the bilayered films, the variations in relative permittivity and tangent loss of each single layered magnetic annealing BFO and reannealing CFO films have been investigated. It is observed that the relative permittivity and tangent loss of BFO and CFO single layer increase and decrease with increasing the applied magnetic field (not show here). The increase in relative permittivity of each single layer is attributed to the reduction in "dead layer" between the different grains boundaries [28]. Thus, the increase in ε_r of the bilayered thin films is ascribed to the reduction in "dead layer". The decrease in tan δ, as shown in the inset of Fig. 3(a), is suggested

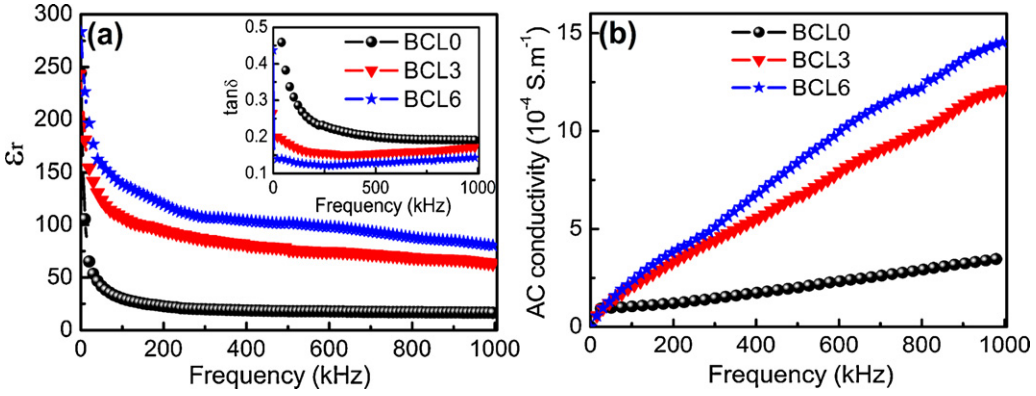

Fig. 3. (a) Frequency dependence of dielectric constant of all the samples. The dependence of the dielectric loss of the films on the frequency is shown in the inset. (b) Frequency dependence of *ac* conductivity of all the films.

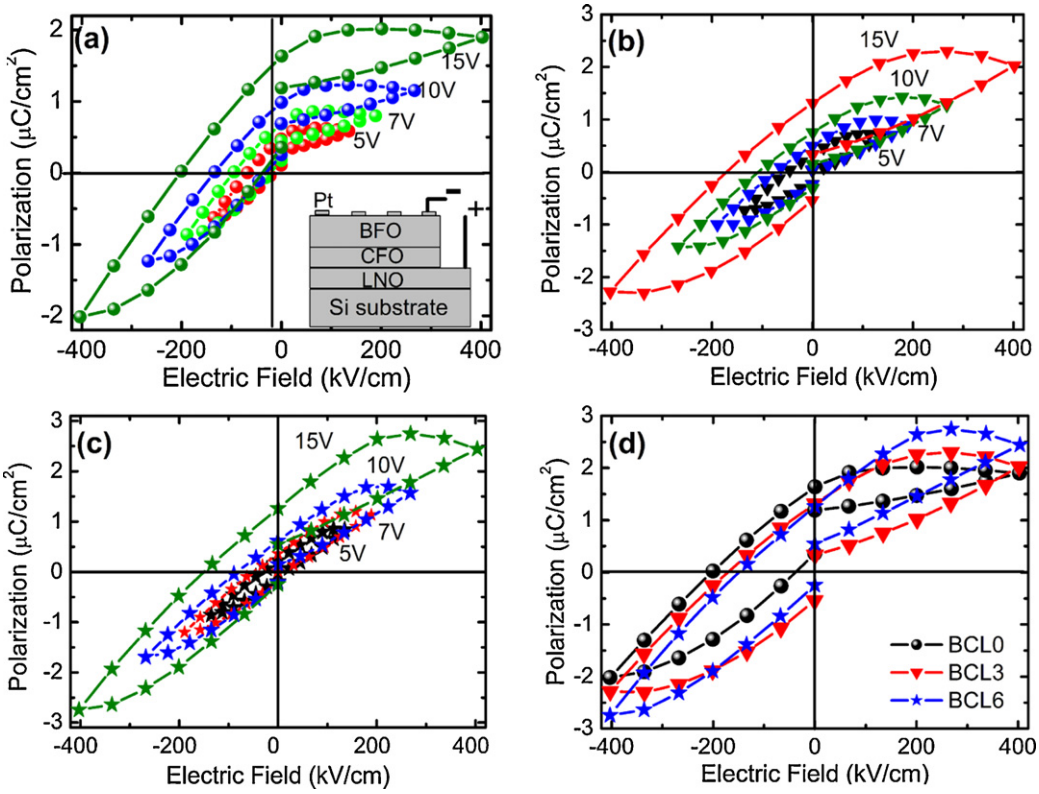

Fig. 4. Room temperature *P–E* hysteresis loops of (a) BCL0, (b) BCL3 and (c) BCL6 measured with increase in maximum voltages of 5, 7, 9 and 15 V at frequency of 2 kHz, with the inset of (a) showing the schematic structure. (d) The *P–E* loops of all the samples measured with maximum voltage 15 V.

to come from the decrease in grain boundary and electrical conduction (leakage current) of BFO and CFO layers due to magnetic annealing, which will be discussed below.

Based on the analysis of the dielectric patterns, *ac* conductivity is calculated from the dielectric data using the relation $\sigma_{ac} = 2\pi\varepsilon_0\varepsilon_r f \tan\delta$, and is plotted in Fig. 3(b), where ε_r is the dielectric constant, $\tan\delta$ is the loss tangent, ε_0 is the permittivity of free space (8.854×10^{-12} F/m) and f is the measuring frequency. As it is known, in many dielectric and ferroelectric materials, the *ac* conductivity of the materials mainly come from the hopping of the polarons and is influenced by the frequency [26,29–32]. From Fig. 3(b), it is seen that the room temperature *ac* conductivity of the bilayered thin films increases with increasing the annealing fields, which originates from the decrease of trap centers such as oxygen vacancies and insulated grain boundaries [29–31]. As the grain boundary and oxygen vacancies reducing, the barrier for hoping carrier decrease, in turn the polarons ever trapped in deep energy level have sufficient thermal energy to jump over the barrier and trapped in shallow energy level can get a long hopping length. As a result, the *ac* conductivity of magnetic annealing films is larger than that of the non-field-annealing films, and increases with increasing the annealing magnetic field. Thus, the increase in relative permittivity and *ac* conductivity as well as decrease in tangent loss of the magnetic annealing bilayered BFO/CFO films is suggested to originate from, at least, the decrease in BFO grain boundary due to magnetic annealing, as shown in Fig. 2.

In order to investigate the magnetic annealing effects on the ferroelectric properties of the bilayered films, measurements of ferroelectric hysteresis are performed with the schematic structure as shown in the inset of Fig. 4(a). Room temperature *P–E* hysteresis loops are measured with increasing maximum voltages at frequency of 2 kHz, and the results are shown in Fig. 4(a)–(c) for BCL0, BCL3 and BCL6, respectively. For giving a clear image of the difference in *P–E* hysteresis loops induced by magnetic annealing, the *P–E* loops of all samples measured with maximum voltage 15 V are plotted in Fig. 4(d). It shows that the remanent polarization of the bilayered films increases with increasing annealing magnetic fields. The improvement in polarization may stem from the increase in strain caused by CFO layers as shown in Fig. 2(c), and decrease in leakage current discussed below. For here the thickness of the BFO layer is no more than 300 nm, and although the polarization hysteresis loops are not saturated and the remanent polarization of our samples is lower compared with other reports [16,17], it is worth noting that the improvement of polarization via magnetic annealing would give a new way to promote the ferroelectric properties for materials preparation. Moreover, better ferroelectric properties of magnetic annealing (1 1 1)-oriented thin films could be expectative, and such works have been in progress.

In addition, for the various electronic applications of films, the leakage current and the conduction mechanism in the thin films are always issues of critical concern. In order to investigate the leakage contribution of the applied magnetic field, the leakage current of all the samples are measured at room temperature within semi-log scale, as shown in Fig. 5(a). It is observed that leakage current in the positive bias voltage region of all the samples is similar to the PLD-derived bilayered BFO/CFO thin films [16], while it is different with the negative bias. The difference in leakage behavior between the positive and negative electric region is attributed to the different work functions of Pt and LNO electrodes [33], and difference in resistivity of BFO and CFO layers [17]. In addition, it is seen that with increasing the annealing magnetic field, the leakage current of the films decreases. In order to further study the magnetic annealing effects on the conduction of the bilayered films, the leakage current curves at positive and negative bias of all samples within log–log scale are plotted in Fig. 5(b) and (c), respectively. It is observed that all the leakage current curves show three straight lines in log–log plots during the measuring bias voltage regions. A power law relationship $\log(I) \sim s \log(V)$ [34–39], is used to fit all the

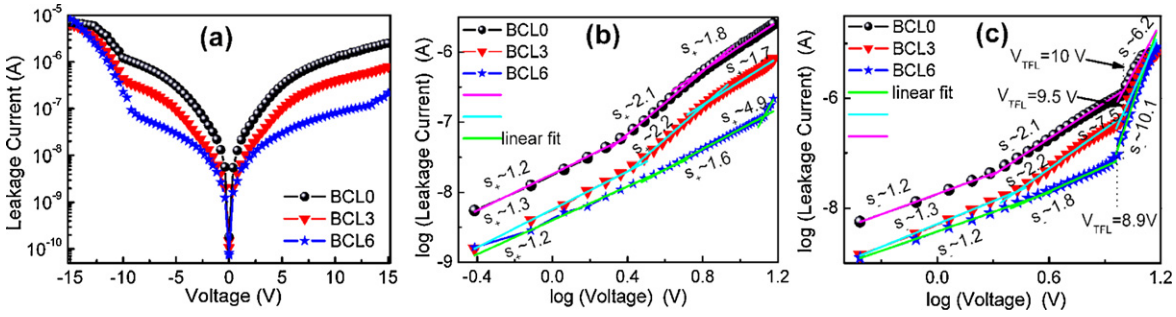

Fig. 5. Variation in the Leakage current of all the bilayered BFO/CFO films with varying bias voltage in (a) semi-log scale, log scale for (b) positive bias and (c) negative bias.

curves shown in Fig. 5(b) and (c). As a result, all the curves are well fitted by three straight lines in log–log plots. It is observed that the value of s is around 1 in the low field regions and around 2 in the middle field regions for both positive and negative voltage regions of all samples, which agrees well with the space-charge-limited current (SCLC) mechanism [37]. In higher electric field region of the positive bias, after SCLC current behavior, the value of s is 1.8 and 1.7 for the BCL0 and BCL3, respectively. The leakage current may be mainly dominated with the SCLC mechanism. However, for the sample BCL6 annealing with 6 kOe field, it shows an abrupt increase in the leakage current with s about 4.9, which is the same behavior as that observed in the high electric field region of negative bias with the value of s about 6.2, 7.5 and 10.1 for BCL0, BCL3 and BCL6, respectively, as shown in Fig. 5(c). The abrupt increase in leakage current may originate from all the available traps becoming filled forced by the applied voltage, which is the trap-filled-limit (TFL) law [39]. The voltage at which this abrupt increase occurs is called trap-filled-limit voltage symbolized with V_{TFL}. It is seen that from Fig. 5(c), the V_{TFL} of the bilayered films decreases from 10 V for BCL0 to 9.5 V for BCL3 and to 8.9 V for BCL6. Since V_{TFL} is determined by the law relationship [39] $V_{TFL} = eN_t d^2/2\varepsilon_r\varepsilon_0$, where N_t is the total trap density, d is the thickness of thin films, e is the electron charge, the decrease in V_{TFL} with increasing annealing magnetic field may be attributed to two aspects. One is the increase in ε_r, as shown in Fig. 3(a). The other may be the decrease in total trap density N_t. It has been reported that oxygen vacancies were related to the origin of space charges in some ferroelectric materials and could create deep-trap energy levels in the band gap for activated electrons to be mobile [32]. In addition, As mentioned in many reports [18,19,23], the presence of oxygen vacancies existing in BFO films can give rise to the appearance of Fe^{2+} which would be the main factor resulting in leakage current. Considering the result shown in Fig. 2, the reduction of the insulator BFO grain boundaries and increase in semiconductor BFO grain [38] should lead to the increase in leakage current of the films with increasing the annealing magnetic field. In fact, the leakage current decrease with increasing the field. Therefore, it could be deduced that the decrease in leakage current of the magnetic annealing films may be attributed to the decrease in oxygen vacancies, which results in decrease in trap center, in turn further give rise to the increase in *ac* conductivity of the films, as shown in Fig. 3(b).

To investigate the effects of magnetic annealing on the magnetic properties of the bilayered BFO/CFO thin films, room temperature magnetic hysteresis loops are measured with the magnetic field parallel to the films surface and shown in Fig. 6. It is observed that all the films exhibit ferromagnetism with a large saturation magnetization. The magnetization of the BFO/CFO bilayered films mainly comes from the ferrimagnetic CFO layer. Although, the saturation magnetization of the bilayered films is lower than that of the single CFO layered thin films, it is much larger than that of single BFO layered films. With the annealing field increasing, the saturated magnetization decreases from 215 emu/cm^3 (BCL0) to 198 emu/cm^3 (BCL3) and to 180 emu/cm^3 (BCL6), as shown in Fig. 6. This change tendency is related to the strain produced in the magnetic annealing process due to large misfit in magnetostriction coefficient between BFO and CFO, just as shown in Fig. 1(c). The strain will clamp the magnetic domain rotating along the direction of the measuring field, and the larger strain and the greater clamped effect. As a result, the saturation magnetization of the bilayered BFO/CFO thin films increases with decreasing magnetic annealing filed. Certainly, the coupling effect existed at the BFO/CFO interface should be considered [17], for the reason of enhancement in BFO (0 0 1)-texture degree as shown in Fig. 1(b).

In order to study the effect of magnetic annealing on the magnetoelectric effects of the BFO/CFO bilayered thin films, the variations of the dielectric constant and dielectric loss with measuring magnetic field are carried out. The variations are characterized by the magnetocapacitance (MC) and magnetolosses (ML) parameters. They are defined as MC (%)=$(\varepsilon_H - \varepsilon_0)/\varepsilon_0 \times 100\%$, and ML (%)=$(\tan\delta_H - \tan\delta_0)/\tan\delta_0 \times 100\%$, where ε_H, $\tan\delta_H$ and ε_0, $\tan\delta_0$ are the dielectric constants and dielectric loss at applied magnetic field and zero field, respectively [40]. Additionally, the MC method is an alternative way of indirectly characterizing the degree of the magnetoelectric coupling effects. The variations of MC and ML values of all the samples versus the measuring magnetic fields paralleled to the films surface and the direction of the applied magnetic annealing field in the range of −40 to 40 kOe measured at 1 MHz, 300 K are plotted in Fig. 7(a) and (b), respectively. The value of negative MC as well as positive ML of field-annealing samples is larger and lower than non-field annealing one. In order to clarify the origins of the MC and ML of the derived bilayered films, the MC and ML of each single layered BFO and CFO had been inves-

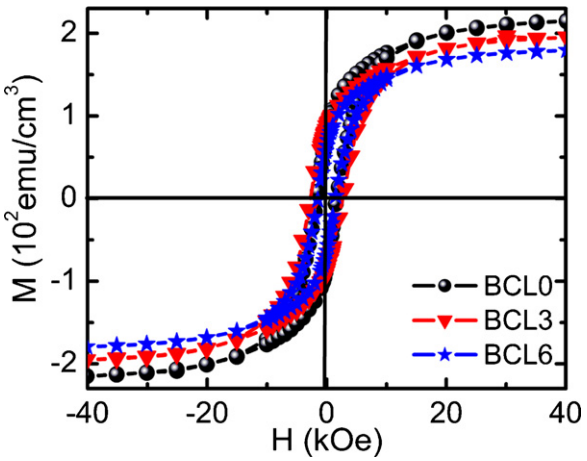

Fig. 6. *M–H* hysteresis loops of the bilayered BFO/CFO thin films with measuring field parallel to the film surface at 300 K.

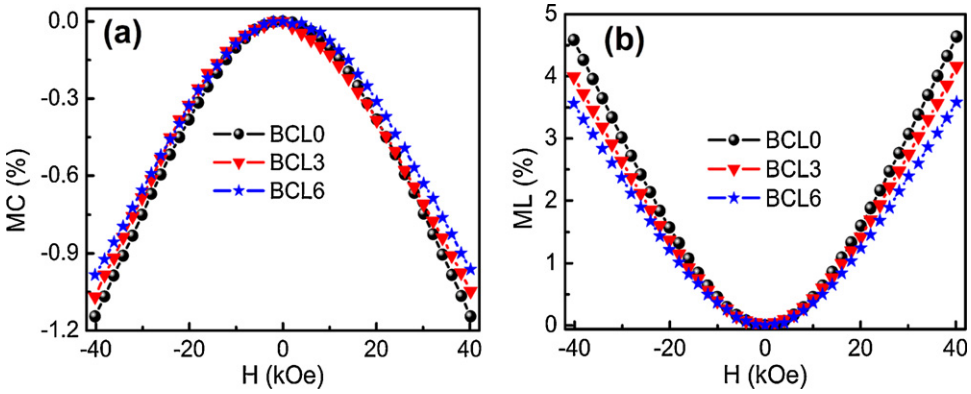

Fig. 7. Magnetic field dependence of (a) magnetocapacitance (MC) and (b) magnetolosses (ML) changes measured with 1 MHz at 300 K of the films.

tigated. It was found that, for the magnetic re-annealing single layered CFO films, negative MC decreases as well as positive ML increases monotonously with the annealing magnetic field, respectively, which is due to magnetoresistance effect combined with the Maxwell–Wagner effect [40]. However, for the single layered BFO films, the magnetic annealing films showed the larger positive MC and lower negative ML due to the enhanced magnetoelectric coupling. These results will be reported elsewhere. Here, the origins of MC and ML may be caused by the cooperation effects of the magnetoresistance effect combined with the Maxwell–Wagner effect, intrinsic magnetoelectric coupling of the BFO layer and the interface coupling between CFO and BFO layer. In addition, increase in MC and decrease in ML suggests the interface coupling enhance with the increasing magnetic annealing fields.

4. Conclusion

In summary, magnetic annealing effects on highly *c* axis-oriented bilayered BFO/CFO thin films by CSD are investigated. The results show that the texture and dielectric constant are enhanced with increasing magnetic annealing fields. The polarization and leakage current increases and decreases with increasing the magnetic field, which provides a new route to improve the ferroelectric properties of BFO films by CSD. Moreover, it is interesting to observe that the magnetocapacitance and magnetoloss increases and decreases with the magnetic annealing fields due to the enhanced the cooperation effects of magnetoresistance effect, Maxwell–Wagner effect, BFO magnetoelectric coupling effect and interface coupling between the BFO and CFO layer.

Acknowledgements

This work was supported by the National Key Basic Research under Contract no. 2007CB925002, the National Science Foundation of China under Contract nos. 10874051 and 50802096, Anhui Provincial NSF Grant no. 070416233, Director's Fund of Hefei Institutes of Physical Science, Chinese Academy of Sciences.

References

[1] H. Béa, M. Bibes, M. Bibes, F. Ott, B. Dupé, X.H. Zhu, S. Petit, S. Fusil, C. Deranlot, K. Bouzehouane, A. Barthélémy, Phys. Rev. Lett. 100 (2008) 017204.
[2] H.W. Jang, S.H. Baek, D. Ortiz, C.M. Folkman, R.R. Das, Y.H. Chu, P. Shafer, J.X. Zhang, S. Choudhury, V. Vaithyanathan, Y.B. Chen, D.A. Felker, M.D. Biegalski, M.S. Rzchowski, X.Q. Pan, D.G. Schlom, L.Q. Chen, R. Ramesh, C.B. Eom, Phys. Rev. Lett. 101 (2008) 107602.
[3] N.A. Spaldin, M. Fiebig, Science 309 (2005) 391.
[4] Y.P. Wang, L. Zhou, M.F. Zhang, X.Y. Che, J.M. Liu, Z.G. Liu, Appl. Phys. Lett. 84 (2004) 1731.
[5] X.W. Tang, J.M. Dai, X.B. Zhu, L.H. Yin, R. Ang, W.H. Song, Z.R. Yang, Y.P. Sun, R.L. Zhang, J. Am. Ceram. Soc. 93 (6) (2010) 1682.
[6] H. Zheng, J. Wang, S.E. Lofland, Z. Ma, L. Mohaddes-Ardabili, T. Zhao, L. Salamanca-Riba, S.R. Shinde, S.B. Ogale, F. Bai, D. Viehland, Y. Jia, D.G. Schlom, M. Wuttig, A. Roytburd, R. Ramesh, Science 303 (2004) 661.
[7] Y. Suzuki, G. Hu, R.B. von Dover, R.J. Cava, J. Magn. Magn. Mater. 191 (1999) 1.
[8] A.P. Chiriac, C.I. Simionescu, J. Polym. Sci. 34 (1996) 567.
[9] D.A. Molodov, P.J. Konijnenberg, Scripta Mater. 54 (2006) 977.
[10] T. Watanabe, S. Tsurekawa, X. Zhao, L. Zuo, Scripta Mater. 54 (2006) 969.
[11] H.L. Niu, Q.W. Chen, H.F. Zhu, Y.H. Lin, X. Zhang, J. Mater. Chem. 13 (2003) 1803.
[12] A.D. Sheikh-Ali, D.A. Molodov, H. Garmestani, Scripta Mater. 46 (2006) 857.
[13] S.X. Dou, W.K. Yeoh, O. Shcherbakova, J. Horvat, J.H. Kim, A.V. Pan, D. Wexler, Y. Li, W.X. Li, Z.M. Ren, P. Munroe, J.Z. Cui, Appl. Phys. Lett. 89 (2006) 202504.
[14] P. de Rango, M. Lees, P. Lejay, A. Sulpice, R. Tournier, M. Lngold, P. Germi, M. Pernet, Nature 349 (1991) 770.
[15] W.J. Lou, D.L. Wang, F.W. Wang, T. Liu, J.W. Cai, L.Y. Zhang, Y.L. Liu, Appl. Phys. Lett. 94 (2009) 202507.
[16] R.Y. Zheng, J. Wang, S. Ramakrishna, J. Appl. Phys. 104 (2008) 034106.
[17] J.G. Wu, J. Wang, J. Appl. Phys. 105 (2009) 124107.
[18] S.K. Singh, H. Ishiwara, K. Maruyama, Appl. Phys. Lett. 88 (2006) 262908.
[19] J.Z. Huang, Y. Wang, Y.H. Lin, M. Li, C.W. Nan, J. Appl. Phys. 106 (2009) 063911.
[20] C.R. Cho, D.A. Payne, S.L. Cho, Appl. Phys. Lett. 71 (1997) 3013.
[21] F.K. Lotgering, J. Inorg Nucl. Chem. 9 (1959) 113.
[22] H. Bea, M. Bibes, S. Petit, J. Kreisel, A. Barthelemy, Philos. Magn. Lett. 87 (2007) 165.
[23] F. Tyholdt, H. Fjellvåg, A.E. Gunnæs, A. Olsen, J. Appl. Phys. 102 (2007) 074108.
[24] M. Kumar, K.L. Yadav, G.D. Varma, Mater. Lett. 62 (2008) 1159.
[25] J.C. Chen, J.M. Wua, Appl. Phys. Lett. 91 (2007) 182903.
[26] J.P. Zhou, H.C. He, Z. Shi, G. Liu, C.W. Nan, J. Appl. Phys. 100 (2006) 094106.
[27] N. Sivakumar, A. Narayanasamy, C.N. Chinnasamy, B. Jeyadevan, J. Phys.: Condens. Matter 19 (2007) 386201.
[28] L.J. Sinnamon, M.M. Saad, R.M. Bowman, J.M. Gregg, Appl. Phys. Lett. 81 (2002) 703.
[29] A. Singh, V. Pandey, R.K. Kotnl, D. Pandey, Phys. Rev. Lett. 101 (2008) 247602.
[30] M. George, S.S. Nair, K.A. Malini, P.A. Joy, M.R. Anantharaman, J. Phys. D: Appl. Phys. 40 (2007) 1593.
[31] J.R. Macdonald, Impedance Spectroscopy Emphasizing Solid Materials and Systems, Wiley, New York, 1987.
[32] J.F. Scott, C.A. Araujo, B.M. Melnick, L.D. McMillan, R. Zuleeg, J. Appl. Phys. 70 (1991) 382.
[33] Z.L. Liu, H.R. Liu, G.H. Du, J. Zhang, K.L. Yao, J. Appl. Phys. 100 (2006) 044110.
[34] M.A. Lampert, Phys. Rev. 97 (1955) 1531.
[35] H. Hu, S.B. Krupanidhi, J. Mater. Res. 9 (1994) 1484.
[36] X. Qi, J. Dho, R. Tomov, M.G. Blamire, J.L.M. Driscoll, Appl. Phys. Lett. 86 (2005) 062903.
[37] M.A. Lampert, P. Mark, Current Injection in Solids, Academic, New York, 1970, p. 23.
[38] A. Rose, Phys. Rev. 97 (1955) 1538.
[39] C. Wang, M. Takahashi, H. Fujino, X. Zhao, E. Kume, T. Horiuchi, S. Sakai, J. Appl. Phys. 99 (2006) 054104.
[40] G. Catalan, Appl. Phys. Lett. 88 (2006) 102902.